BEAM POSITION MONITORING

Robert E. Shafer
Los Alamos National Laboratory, Los Alamos, NM 87545

1. INTRODUCTION

The purpose of this paper is to review the topic of beam position monitoring as it applies to charged-particle beams in accelerators and beamlines. As this workshop is primarily to familiarize engineers with the subject, the emphasis will be on the engineering aspects of beam position measurement rather than on pedantic derivations of equations. The intent is not to present many specific solutions to specific problems, but to provide general guidelines on which specific designs can be based, with occasional examples. Some math must be included, however, to understand how pickup electrodes respond to beams and how various circuits process signals. The emphasis will be on calculating frequency dependence, power levels and beam-displacement sensitivities, and reviewing the advantages and disadvantages of a variety of electrode designs and signal-processing methods.

Beam instrumentation includes not only the electronics necessary to measure the properties of beams, but also the transducers that convert the beam signals into electrical signals. Processing electrical signals is a very well understood engineering field. The characteristics of the transducers that generate the electrical signals are not well documented, however. There is quite a bit of physics in beam transducers, and because the beam currents are not confined to wires, engineers sometimes have difficulty grasping the basic concepts in how particle beams couple to beam diagnostic devices and generate electrical signals. Therefore, this paper will concentrate on the beam-coupling mechanism, but will also discuss some of the signal-processing electronics.

First, the basic methods of noninterceptive beam position monitoring will be discussed. Then the basic characteristics of beams and beam position measuring systems will be reviewed. This is followed by several sections that discuss the signals from a variety of pickup electrode geometries. Several sections are then devoted to signal processing methods. Finally, several sections discuss the system aspects of beam position monitoring.

There have been several comprehensive survey articles on beam diagnostics stressing primarily the physics aspects of the subject.[1-6] These articles cover the broad range of particle beam diagnostics and are not restricted to position measurement.

2. BASIC METHODS OF BEAM POSITION MONITORING

The most common method of monitoring the position of a charged-particle beam is to couple to the electromagnetic field of the beam. The beam is a current, and it is therefore accompanied by both a magnetic field and an electric field. In the limit of very high beam energy, the fields are pure transverse electric and magnetic (TEM). If the beam is displaced from the center of a hollow

conducting enclosure, the magnetic and electric fields are modified accordingly. Detailed knowledge of how the magnetic and electric fields depend on the beam position allow accurate determination of the beam position.

Pickup electrodes, in general, cannot sense dc electric or magnetic fields (there are exceptions to this, of course, such as Hall probes and flux-gate magnetometers). The signals are induced by a time-varying component of the beam signal, usually beam current modulation. The carrier for the beam position information is the frequency (and harmonics) of the periodic beam bunches for a continuous train of bunches or the derivative of the instantaneous beam current for single bunches.

The conventional beam position pickup is a pair of electrodes (or two pair, if two beam position coordinates are being measured) on which the signals are induced. The ratio of the amplitudes of the induced signals at the carrier frequency is uniquely related to the beam position. Because the position information is contained in the amplitude variation of these signals, the information actually appears as AM (amplitude modulation) sidebands of the carrier. In synchrotrons, where the strong focusing forces cause the betatron oscillation frequency to be many times the revolution frequency, the sidebands are substantially displaced in frequency from the carrier signal.[3,4]

A variant of the standard multielectrode beam position monitor is the wall-current monitor,[7] which often is a gap in the beam pipe with a ceramic insert to maintain vacuum. A resistive path, often composed of many resistors in parallel, is connected across the gap to carry the wall currents. The azimuthal distribution of wall currents, determined by measuring the voltage drop across the resistors, can be used as a measurement of the beam position.

Another nearly noninterceptive method of measuring position is to intercept the beam with objects such as thin wires and to measure the response of the wire (induced currents) or ionizing radiation produced by the beam hitting the wire as the wire is moved through the beam.[8] The wire, usually a low-Z material, may be either stepped through the beam or pushed through at a high velocity.[8] In either case, some of the beam is lost or scattered out of the incident beam, causing some degradation of the beam quality. In addition, the wire is heated by the beam and, in many cases, is damaged by being overheated.

Still another method is to cause the beam itself to radiate energy. High-energy electrons, when they pass through large magnetic fields, will radiate visible, uv light or x-rays in narrow forward cones (synchrotron radiation). Detectors designed to intercept this synchrotron radiation can be used to determine the position of the source (i.e., the beam) in the magnetic field.[9] This general technique is used in electron synchrotrons (synchrotron light sources) and in devices such as wigglers and undulators, which are specifically designed to make the electrons radiate.

Residual gas fluorescence[10] or ionization[11] can be used to determine beam position. In the former, video-image processing of the visible light is used to determine the beam profile and position. In the latter, an electric field

perpendicular to the beam is used to accelerate the liberated electrons or ions to a detector.

Finally, it is possible to probe the beam with another beam, and monitor the radiation produced by the two interacting beams. At the Stanford Linear Accelerator Center, for example, two very high energy beams (one an electron beam and the other a positron beam), are directed toward each other in the collision (final focus) area of the Stanford Linear Collider (SLC). [12,13] The magnetic fields of each beam cause the other beam to be deflected and radiate (beamstrahlung). Measurement of the radiation yield as a function of the relative position of the two beams leads to a measurement of the relative beam positions.

In the case of negative-ion beams such as H^- (a proton with two electrons attached), a thin visible laser beam (photon energy about 2 eV) can be used to detach one of the electrons[14] (the binding energy of the "extra" electron is about 0.75 eV). The result is that a narrow beam of neutral hydrogen atoms is produced. By monitoring the yield of the neutral hydrogen as a function of the position of the laser beam, the beam position can be determined. Laser beams may also be scattered off high-intensity electron beams as a probe.[15]

There are many ways of determining the beam position in a nearly noninterceptive way. The best one is determined by the type of beam being monitored, the conditions under which the monitoring is being done, and, finally, what specific measurements are required. Because the most common noninterceptive method is measuring the electric and magnetic fields, the remainder of the paper will discuss this method.

3. CHARACTERISTICS OF BEAMS AND POSITION MEASURING SYSTEMS

The purpose of this section is to discuss some of the beam and beam position measuring system characteristics that need to be considered when such a system is being designed. It is important to understand the range of the beam parameters to be expected and the requirements of the beam position monitoring system before undertaking a detailed design of the system. It is nearly always true that some compromises must be made in order to go from an ideal system design to a realizable one. These compromises may be due to time constraints, funding, space, or manpower resources. Hence, it is important to have a thorough understanding of how each parameter affects, or is affected by, the system design. With this understanding, it is usually possible to design a system that is simple, yet does not compromise the quality of the measurements.

Accuracy is the ability to determine the position of the beam relative to the device being used for measuring the beam position. This is limited by some combination of mechanical alignment errors, mechanical tolerances in the beam detection device, calibration errors in the electronics, attenuation and reflections in the cables connecting the pickup to the electronics, electromagnetic interference, and circuit noise (noise figure of the electronics). Signal processing

introduces additional inaccuracies such as granularity (least-significant-bit [LSB] errors) that is due to analog-to-digital conversion.

Resolution differs from accuracy in that it refers to the ability to measure small displacements of the beam, as opposed to its absolute position. Typically, the resolution of a system is much better than the accuracy. In many cases, good resolution is much more important than good accuracy. For example, it is often adequate to know the absolute beam position to a fraction of a millimeter, even though the beam motion (jitter) needs to be known to a few micrometers. In high-energy collider operation, for example, it is much more important to know the relative position of the two beams than to know the absolute position of either.

Bandwidth refers to the frequency range over which beam position can be measured. In some cases, a beam may have a fast transverse motion (jitter) that needs to be identified. In another case, the beam pulse may be very short (a picosecond, nanosecond, or a microsecond for example), and the measuring system must be able to acquire data in this time interval (acquisition bandwidth). Closely related is real – time bandwidth, which is the ability to generate a real-time analog signal proportional to the beam position in a limited time. This response is necessary if the signal is to be used in real-time, closed-loop control applications.

Beam current usually refers to the average (dc) beam current averaged over the microscopic bunch structure, but can also be used to refer to the instantaneous (intrabunch) beam current and to other temporal averages. For single bunches, the number of particles per bunch is often used as a measure of beam current. Closely related is beam intensity, which usually refers to the amplitude of a particular frequency harmonic of the beam-bunching frequency. Beam intensity differs from beam current in that intensity is a frequency-domain quantity, while current is a temporal-domain quantity.

Dynamic range refers to the range of beam intensities (or current or charge) over which the diagnostic system must respond. Often large dynamic range response is achieved by gain switching, but in addition, special methods of signal processing can provide a large dynamic range response and eliminate the need for gain switching.

Signal – to – noise ratio refers to the relative power levels of the wanted signal to unwanted noise. Noise may be true thermal noise, amplifier noise (noise figure), electromagnetic noise (EMI) such as silicon-controlled-rectifier (SCR) noise, or radio-frequency interference (RFI), which may be the same frequency as the beam position signals. In this application, shot noise (sometimes called Schottky noise) from the beam itself is actually a signal, because it can be used to determine the beam position. Signal-to-noise ratios place limits on the ultimate resolution of the system.

Beam bunching refers to the temporal characteristics of the beam current modulation. Usually the beam is in the form of short bunches with the same period as, or a multiple of, the period of the rf system being used to accelerate it. For example, at the Los Alamos Meson Physics Facility (LAMPF), the bunch

period is about 5 ns (201.25 MHz), while the rf period is 1.25 ns (805 MHz). The bunch length is usually quite short relative to the period and at some facilities is less than 30 ps. The bunch shape can be temporally symmetric such as Gaussian, parabolic, or cosine-squared, among others. It can also be nonsymmetric. The beam-bunching factor is typically the ratio of the bunching period to the beam bunch full length at half maximum (F L HM). Typically, this factor can be 10 or 20, often higher. This temporal profile creates many harmonics of the bunching frequency in the induced signals on the pickup electrodes. Beam bunching can change with time because of momentum spread in a nonisochronous beam-transport system, synchrotron oscillations in rf buckets, or by allowing a space-charge-dominated beam to coast in a beamline without longitudinal focusing forces.

4. BEAM CURRENT MODULATION IN THE TIME AND FREQUENCY DOMAINS

Beam bunches can have many shapes. Regardless of what the specific shape is, the beam-bunching frequency usually provides the carrier signal that is used for detecting the beam position. Because it is possible to make measurements in either the time or frequency domain, it is important to understand the interrelations between the two cases. A Gaussian bunch shape is used in the following calculations, although other shapes could just as easily have been used.

Consider a Gaussian-shaped beam bunch containing N particles of charge e in a bunch of rms temporal length σ (in time units) and with a bunching period T. The instantaneous beam current of a single bunch is given by

$$I_b(t) = \frac{eN}{\sqrt{2\pi}\sigma}\exp\left[\frac{-t^2}{2\sigma^2}\right] \quad . \tag{4.1}$$

This is normalized so that the bunch area is the total charge eN independent of the rms bunch length σ. Assuming that the bunch is symmetric in time, centered at $t = 0$, and is in a pulse train with bunch spacing T, we can expand this in a cosine series with $\omega_0 = 2\pi/T$:

$$I_b(t) = \frac{eN}{T} + \sum_{m=1}^{\infty} I_m \cos\left(m\omega_0 t\right) \quad , \tag{4.2}$$

where

$$I_m = \frac{2eN}{T}\exp\left[\frac{-m^2\omega_0^2\sigma^2}{2}\right] \quad . \tag{4.3}$$

This may be rewritten

$$I_b(t) = \langle I_b\rangle + 2\langle I_b\rangle \sum_{m=1}^{\infty} A_m \cos\left(m\omega_0 t\right) \quad , \tag{4.4}$$

where the average (dc) beam current is

$$\langle I_b \rangle = \frac{eN}{T} \quad , \tag{4.5}$$

and the harmonic m amplitude factor is

$$A_m = \exp\left[\frac{-m^2\omega_0^2\sigma^2}{2}\right] \quad . \tag{4.6}$$

The Fourier cosine series expansion of the beam current in Eq. (4.4) includes a dc component as well as many harmonics of the bunching frequency. The amplitude (intensity) of the various Fourier harmonics is determined by the factor A_m, which always approaches 1 for small harmonic numbers, regardless of the specific bunch shape. As the bunch shape approaches a δ function, the amplitude factor A_m approaches 1 for all harmonics. The peak amplitude of the low harmonics of the bunching frequency is about twice the dc current. Table 4.1 gives the amplitude factor A_m for a variety of pulse shapes.

Table 4.1. Amplitude factor A_m for a variety of bunch shapes. All expressions are normalized so that $A_m \to 1$ as the bunch length $\to 0$. In the table, T is the bunch spacing, W = full width at base of bunch, and $\omega_0 = 2\pi/T$.

Bunch Shape	A_m	Comment
δ function	1	For all harmonics
Gaussian	$\exp\left(\frac{-m^2\omega_0^2\sigma^2}{2}\right)$	σ is rms bunch length
Parabolic	$3\left(\frac{\sin\alpha}{\alpha^3} - \frac{\cos\alpha}{\alpha^2}\right)$	$\alpha = m\pi W/T$
$(\text{cosine})^2$	$\frac{\sin(\alpha-2)\pi/2}{(\alpha-2)\pi} + \frac{\sin\alpha\pi/2}{\alpha\pi/2} + \frac{\sin(\alpha+2)\pi/2}{(\alpha+2)\pi}$	$\alpha = 2mW/T$
Triangular	$\frac{2}{\alpha^2} - \frac{2\cos\alpha}{\alpha^2}$	$\alpha = m\pi W/T$
Square	$\frac{\sin\alpha}{\alpha}$	$\alpha = m\pi W/T$

It should be noted that many bunch shapes can have zero values of A_m for certain harmonics m of the bunching frequency, depending on the bunch length. If a beam position system is being designed to operate at a harmonic of the bunching frequency, this must be taken into account. If the bunch shape is

variable, then the amplitude factor may vary and may even go to zero, depending on the specific bunch shape and length.

In summary, the currents associated with periodically spaced beam bunch may be considered either in the time domain or the frequency domain. Generally, if the signal processing is performed at harmonic m =1 in the frequency domain, the amplitude factor A_1 is nearly 1, and the rms beam intensity at this frequency is $\sqrt{2}$ times the dc current.

An interesting alternate method to using the rf bunching modulation is the beam current modulation scheme being planned at CEBAF. A 1-μA rms beam current modulation at 10 MHz is placed on the 200-μA cw electron beam[16] (rf frequency is 1497 MHz). Because the 10-MHz modulation can be turned on for less than one revolution around the recirculating linac (period about 4.2 μs), it is possible to measure the position of individual orbits while the machine is in operation. There are two other advantages to this method: First, the instrumentation is less expensive at 10 MHz, and second, the modulation scheme can be used without adversely affecting running experiments.

If a beam is centered in a circular, conducting beam pipe of radius b and has a velocity $v_b = \beta_b c$ (where c is the speed of light), then there is an electromagnetic field accompanying the beam and an equal magnitude, opposite charge, uniformly-distributed beam current density on the inner wall of the beam pipe. The field inside the beam pipe looks (nearly) like a transverse-electric-magnetic (TEM) wave propagating down the beam pipe at the beam velocity (this is exact only for $\beta_b = 1$). Beam position detectors sense these fields (or, equivalently, the corresponding wall current) and determine the beam position based on the relative amplitudes of the induced signals in two or more pickup electrodes. The instantaneous Fourier harmonic amplitudes of the wall currents (integrated over 2π), in this case, are the same as those for the beam itself. The wall current density is then, for a beam pipe with infinite conductivity, simply the beam current divided by the beam-pipe circumference:

$$i_w(t) = \frac{-I_b(t)}{2\pi b} \tag{4.7}$$

Some authors like to differentiate between pickups that detect the TEM fields and those that sense the wall currents. There is no difference. For a beam current $I_b(t)$ in the center of a conducting beam pipe of radius b, the azimuthal magnetic field accompanying it is $H_\theta(r,t) = I_b(t)/2\pi r$. Because $[\text{curl } \mathbf{H}(t)]_z = J_z(t)$, the discontinuity of $H_\theta(r,t)$ at $r = b$ requires that $J_z(b,t) = H_\theta(b,t)$, as long as the magnetic fields associated with the beam are confined to the region inside the beam pipe. For this reason, we can consider either the TEM wave or the wall current density as the excitation signal. For an rf-modulated cw beam in a metallic beam pipe, the magnetic field associated with the dc component of Eq. (4.4) will eventually appear outside the beam pipe, and the wall currents will then include only the ac components.

Circular beam pipes are the most common shape, and so the rest of this paper will deal exclusively with circular geometry. Other geometries for beam pipes

and beam pickup electrodes include rectangular, diamond, and elliptical, among others. All the calculations carried out in this paper can be done for these other geometries, with similar results.

5. SIGNALS FROM OFF-CENTER BEAMS

In the previous section, we considered a centered beam in a circular beam pipe. We now investigate what happens to the wall currents when the beam is displaced from the center.

LaPlace's equation can be solved in two dimensions to find the wall current density for a pencil beam current I_b(t) at position r, θ inside a grounded, circular, conducting beam pipe of radius b.[17] The wall current density i_w at b, ϕ_w is then

$$i_w(b, \phi_w, t) = \frac{-I_b(t)}{2\pi b}\left[1 + 2\sum_{n=1}^{\infty}\left(\frac{r}{b}\right)^n \cos\left[n(\phi_w - \theta)\right]\right] . \qquad (5.1)$$

An alternate way to obtain a solution is to use the method of images. In this case, the location of an image pencil beam is found such that the potential everywhere on the circle corresponding to the beam-pipe location (without the beam pipe) is zero. The wall current is then calculated using the differential form of Gauss's Law (div $\mathbf{E} = \rho/\epsilon_0$). The resultant expression for the wall current density i_w at b, ϕ_w is [18]

$$i_w(b, \phi_w, t) = \frac{-I_b(t)}{2\pi b}\left[\frac{b^2 - r^2}{b^2 + r^2 - 2br\,\cos\,(\phi_w - \theta)}\right] . \qquad (5.2)$$

This closed-form expression, which is equivalent to the infinite series form in Eq. (5.1), is sometimes easier to deal with than the infinite series. However, when the expression must be integrated, the infinite series is often the preferred form. Note that the infinite series is of the form $r^n \cos n\theta$, indicative of solutions in cylindrical geometry.

If two electrodes (L and R for left and right) of angular width ϕ are placed at 0° and 180°, as shown in Fig. 5.1, the resultant currents flowing parallel to the beam on the inside surface of these electrodes are (assuming they are grounded and also at radius b)

$$I_R(t) = \frac{-I_b(t)\phi}{2\pi}\left\{1 + \frac{4}{\phi}\sum_{n=1}^{\infty}\frac{1}{n}\left(\frac{r}{b}\right)^n \cos\,(n\theta)\,\sin\left(\frac{n\phi}{2}\right)\right\} , \qquad (5.3)$$

and

$$I_L(t) = \frac{-I_b(t)\phi}{2\pi}\left\{1 + \frac{4}{\phi}\sum_{n=1}^{\infty}\frac{1}{n}\left(\frac{r}{b}\right)^n \cos\,(n\theta)\,\sin\left[n\left(\pi + \frac{\phi}{2}\right)\right]\right\} . \qquad (5.4)$$

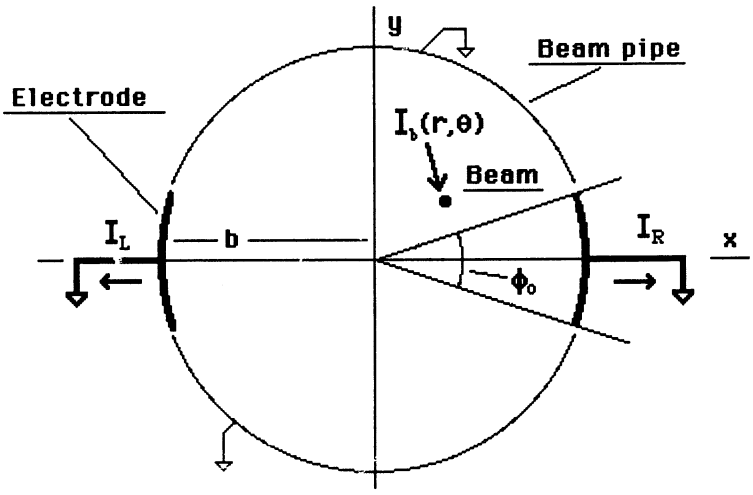

Fig. 5.1. Cross section of beam position monitor pickup model used for calculations.

$$\frac{R-L}{R+L} = \frac{4\sin(\phi/2)}{\phi}\frac{x}{b} + \text{ higher order terms} \quad . \tag{5.5}$$

A more linear (in x) approximation in cylindrical geometry is to write the ratio of R/L in decibels (i.e., logarithmic form):

$$20\ \text{Log}_{10}\left(\frac{R}{L}\right) = xS_x = \frac{160}{Ln\ 10}\frac{\sin(\phi/2)}{\phi}\frac{x}{b} + \text{ higher order terms} \quad . \tag{5.6}$$

As an example, consider two opposing 36° ($\phi = 0.63$) electrodes in a 27.5-mm radius beam pipe. The calculated sensitivity S_x is 1.25 dB per millimeter of displacement. This sensitivity, multiplied by the displacement x, gives the decibel difference of the two signals. If the displacement is 10 mm, for example, the decibel difference is about 12.5 dB, corresponding to an amplitude ratio of 4.2 to 1.

In actuality, the electrodes are neither grounded nor at the same radius as the beam pipe. In practice, the best empirical results are obtained if the radius used in Eq. (5.6) is the average of the electrode and the beam pipe radius. As an example, consider the Deutches Electronen Synchrotron Laboratory (DESY) directional coupler beam position pickup,[19] which has electrode dimensions corresponding to the above example and a ground plane radius of 32.5 mm.

The calculated sensitivity for a 30-mm effective-radius aperture is 1.14 dB per mm, which is close to the measured sensitivity of 1.18 dB per mm.

The actual measured response of the DESY pickup is a nonlinear function of displacement. Figure 5.2 shows the calculated response for a displaced beam in this geometry, using the decibel ratio of Eqs. (5.3) and (5.4). This curve agrees very well with the actual response.[19]

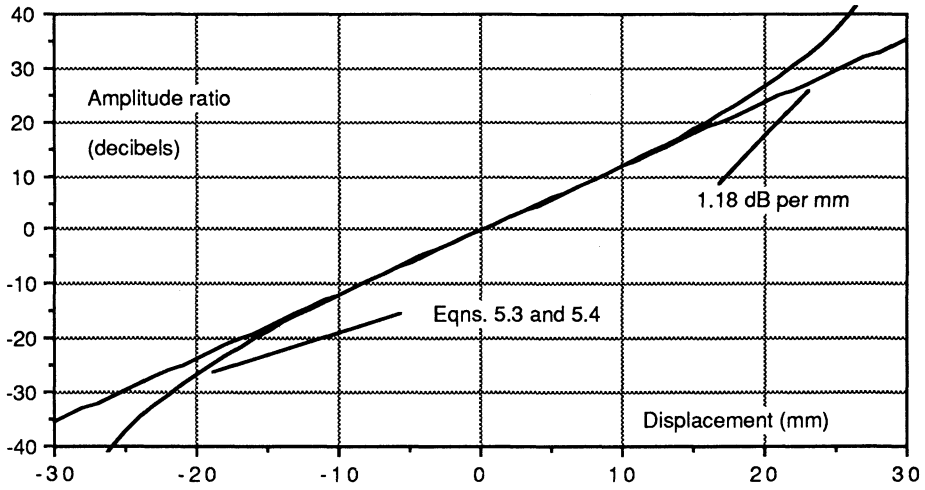

Fig. 5.2. Amplitude ratio response for a beam position monitor with a 60-mm-diam aperture and 36° electrodes. The calculated response using Eqs. (5.3) and (5.4) agrees closely with actual measurements.

Figure 5.3 shows the calculated integral linearity S_x (output amplitude divided by the x displacement) for this pickup for a vertically centered ($y = 0$), horizontally displaced beam and also for a beam displaced vertically by $y = \pm 10$ mm, using Eqs. (5.3) and (5.4). Due to the y-plane dependence, the variation of S_x inside a 20-mm-diam circle is about $\pm 7\%$.

In general, the pickup displacement sensitivity S_x is dependent on both the in-plane and orthogonal-plane displacements x and y. The in-plane nonlinearity can be corrected after the measurement using a software algorithm or look-up table. The orthogonal plane nonlinearity cannot be corrected, however, unless the y position is also measured.

Special electrode geometries can minimize this effect. As an example, Fig. 5.4 shows the calculated response for the above pickup with the electrode width increased to 75°. In this case, the y-plane nonlinearity is nearly zero, and S_x is flat within about $\pm 2\%$ inside a 20-mm-diam circle.

Both Eqs. (5.5) and (5.6) for the electrode response to a beam displacement have higher-order terms and therefore are nonlinear. The nature of the

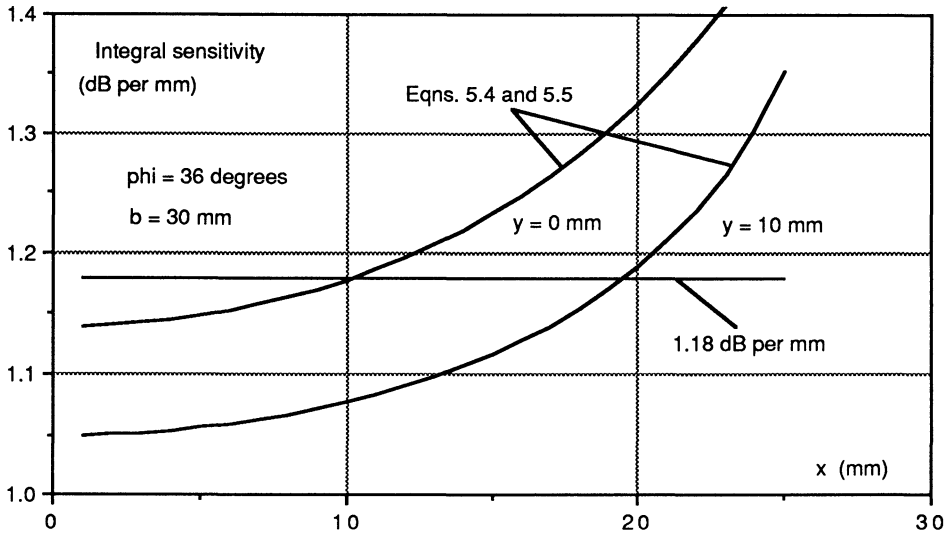

Fig. 5.3. Integral linearity plot for the pickup in Fig. 5.2 (60-mm-diam aperture with 36° electrodes). Note that the sensitivity for a vertically displaced beam ($y = \pm 10$ mm) is about 10% lower than for a vertically centered beam.

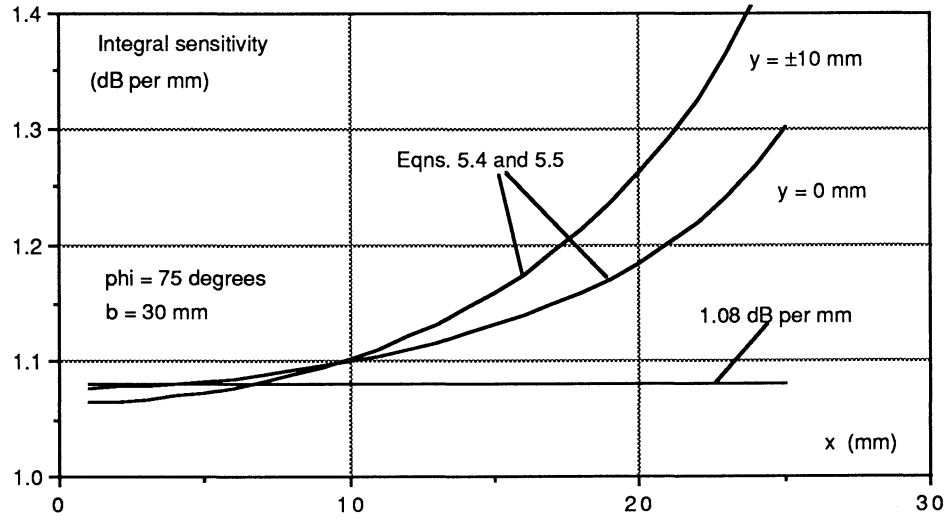

Fig. 5.4. Integral linearity plot for a pickup with a 60-mm-diam aperture and 75° electrodes. Note that the sensitivity for a vertically displaced beam ($y = \pm 10$ mm) is nearly the same as for a vertically centered beam.

nonlinearities are different for the two expressions, however, because Eq. (5.5) represents the normalized difference and Eq. (5.6) represents the logarithmic ratio. It is possible to design an electrode shape that is linear in the normalized difference, and this design will be discussed in a later section.

6. ELECTROSTATIC PICKUP ELECTRODES

We first consider the response of electrostatic (sometimes called capacitive) pickups. We consider specifically two opposing electrodes of length ℓ and azimuthal width ϕ in a beam pipe of radius b. If the current of a centered pencil beam is I_b(t) and the beam has velocity $v_b = \beta_b c$, the charge density of the beam is

$$q_b(t) = \frac{I_b(t)}{\beta_b c} \quad . \tag{6.1}$$

Equal magnitude, opposite-polarity charge appears on the inside surface of the electrodes. For an electrode of length ℓ and azimuthal width ϕ, this charge is

$$Q_s(t) = \frac{-\phi\ell}{2\pi}\frac{I_b(t)}{\beta_b c} \quad . \tag{6.2}$$

Assuming there is capacitance between the electrode and ground given by C, the signal current flowing onto the capacitance is equal to the time derivative of the charge on the electrode:

$$i_s(t) = \frac{-dQ_s(t)}{dt} = \frac{\phi\ell}{2\pi}\frac{1}{\beta_b c}\frac{dI_b(t)}{dt} \quad . \tag{6.3}$$

Note that there is no dc component of charge on the capacitance. The capacitance integrates this current, yielding an output voltage

$$V_c(t) = \frac{\phi\ell}{2\pi C}\frac{I_b(t)}{\beta_b c} - V_0 \quad , \tag{6.4}$$

where V_0 is a constant of integration.

This capacitance may be directly between the electrode and the beam pipe, or it may be added externally. The equivalent circuit is shown in Fig. 6.1. It is important to note that the signal source is a current source, and that there is some inter-electrode capacitance. In addition, there is a bleeder resistor used to prevent excessive charge build-up in the circuit. The bleeder resistor causes the average voltage on the capacitor to be zero. Usually in electrostatic pickup circuits the shunt capacitance is the dominant conductance path at the important frequencies, and the voltage across it then represents the beam bunch temporal profile, as is seen in Eq. (6.4).

As an example, consider an electrostatic pickup electrode in the Proton Storage Ring (PSR) at the Los Alamos Meson Physics Facility (LAMPF). With a bunched 20-A peak current of 800-MeV protons ($\beta_b = 0.84$), an electrode of

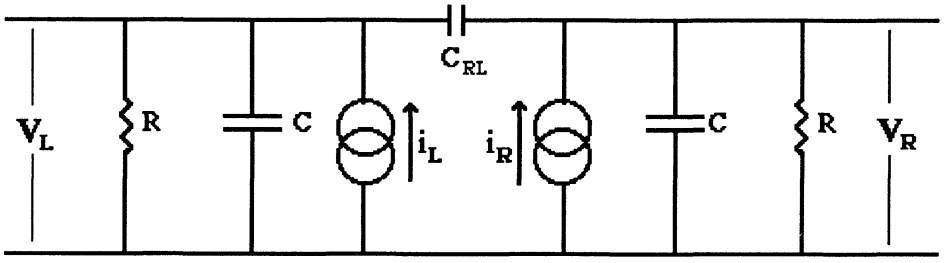

Fig. 6.1. Equivalent circuit for an electrostatic pickup. The signal sources are current generators with amplitudes specified in Eq. (6.3). Note that there is also an interelectrode coupling capacitance.

120° width and 10-cm length, and a capacitance-to-ground of 2 nF, the peak-to-peak output voltage is 1.3 V.

Usually these electrodes are coupled to the electronics by a short piece of transmission line. If neither end is properly terminated, then it is possible to excite standing waves in the cable. For this reason, special effort must be taken to damp the standing waves. The problem is most serious if the electronics is remote from the beam line, either because of the desire to have it outside the interlocked area, or to prevent radiation damage. Sometimes rad-hard electronics (in the form of a cathode follower[20]) can overcome the radiation problem.

7. LINEAR RESPONSE PICKUP ELECTRODE DESIGN

We now consider a hollow tube with radius b and length 2L inside a grounded beam pipe. If the tube is cut diagonally to make two electrodes as shown in Fig. 7.1, the response to beam displacement is linear. This can be seen as follows.

If a beam of charge density q_b is displaced an amount r, θ from the axis of a cylinder whose length is given by $L(\phi) = L(1 + \cos\,\phi)$, the total charge on the inner surface of the cylinder is

$$Q_s = -q_b L \int_o^{2\pi} \frac{(1 + \cos\,\phi)(b^2 - r^2)}{b^2 + r^2 - 2br\,\cos\,(\phi - \theta)} d\phi \quad . \tag{7.1}$$

Upon integration (with some difficulty), this becomes

$$Q_s = -q_b L\left(1 + \frac{r\,\cos\,\theta}{b}\right) = -q_b L\left(1 + \frac{x}{b}\right) \quad , \tag{7.2}$$

which is linear in the beam displacement. The dispacement sensitivity S_x is then given by

$$\frac{R - L}{R + L} = \frac{x}{b} \quad , \tag{7.3}$$

which is only half the sensitivity of the electrodes in Eq. (5.5).

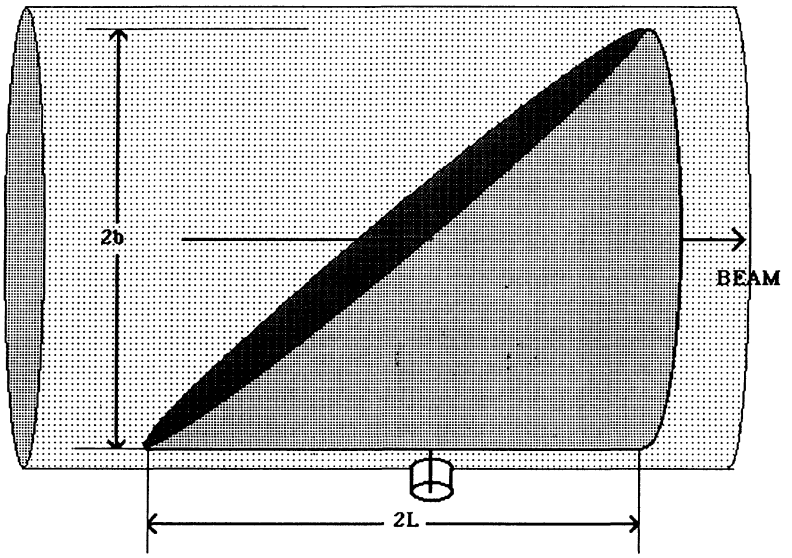

Fig. 7.1. Side view of a diagonally cut circular cross-section electrode that produces a linear response to a displaced beam. The displacement sensitivity (in decibels per unit displacement) is about 50% of a directional coupler with similar aperture.

8. BUTTON ELECTRODES

Button electrodes,[21] in common use around electron synchrotrons and storage rings, are a variant of the electrostatic electrode. The electrodes are very small and usually circular. Unlike the electrostatic electrode, however, the transmission line carrying the output signal to the electronics is terminated in its characteristic impedance, thus giving a differentiated signal. Their equivalent circuit is essentially Fig. 6.1, but with R being the terminating resistance and C being very small. Using a radius b for the beam-pipe half-aperture, the voltage onto a termination of R Ω is, using Eq. (6.3):

$$V_B(t) = R\, i_s(t) = \frac{\phi \ell R}{2\pi\beta_b c}\,\frac{dI_b(t)}{dt} \quad . \tag{8.1}$$

For circular elecrodes, the factor $\phi\ell$ should be set equal to the electrode area divided by b.

It is useful to combine Eq. (8.1) with Eq. (4.1) to calculate the button-electrode response to a single Gaussian beam bunch containing N particles (for $\sigma > \ell/\beta_b c$):

$$V_B(t) = \frac{-eN}{(2\pi)^{3/2}} \frac{\phi \ell R}{\beta_b c} \frac{t}{\sigma^3} \exp\left[\frac{-t^2}{2\sigma^2}\right] \quad . \tag{8.2}$$

The peak output voltage of this bipolar doublet, which occurs at about $t = \pm\sigma$, is then given by

$$V_{\text{peak}} = \frac{eN}{(2\pi)^{3/2}} \frac{\phi \ell R}{\beta_b c} \frac{e^{-1/2}}{\sigma^2} \quad . \tag{8.3}$$

This peak amplitude varies inversely as the square of the beam bunch length. For this reason, button electrodes are most useful around machines with very short bunches (i.e., electron accelerators and storage rings) and are not normally used around proton machines, which typically have longer bunch lengths (an exception to this is the PETRA ring at DESY, which will use button electrodes for monitoring both electron and proton beams).

If we use Eq. (8.1) in combination with the Fourier series expression as shown in Eq. (4.4), the rms output voltage for a beam intensity signal at frequency $\omega/2\pi$ is (where $A(w)$ is the amplitude factor Eq. (4.6) at frequency w)

$$V_B(\omega) = \frac{\sqrt{2}\phi R}{\pi} \langle I_b \rangle \, A(\omega) \frac{\omega \ell}{2\beta_b c} \quad . \tag{8.4}$$

This signal amplitude rises linearly with frequency for a given average beam current.

9. RESONANCES IN PICKUP ELECTRODES

We now consider a simple electrostatic electrode inside the beam pipe, as shown in Fig. 9.1. Assuming the only external connection to the electrode is at the center, both the upstream and downstream ends of the electrode are open (i.e., unterminated). Because the electrode forms a transmission line with the beam-pipe wall behind it and has a capacitance and an inductance per unit length, the electrode can resonate with current nodes at each end. Any resonance that has a voltage node at the external connection will resonate with a high Q, because no power can be coupled into the external circuit. The voltage induced by the passing beam thus remains on the electrode and, in some instances, can lead to beam instabilities. For this reason, electrostatic-type pickups of any shape should be avoided if possible. An exception is the button electrode, which is so short that the resonances are at very high frequencies (tens of GHz).

One way to couple to all the resonances in pickups is to make the external signal attachment at one end. In this way all resonances will couple to the external circuit. If, however, the transmission line used for the external circuit has a different characteristic impedance than the electrode itself, there will be a voltage-standing-wave ratio (VSWR) at the connection, and several reflections will be required for the power on the electrode to escape onto the transmission line. This will distort the temporal response of the electrode, which is a concern if the electrode is to be used at high frequencies.

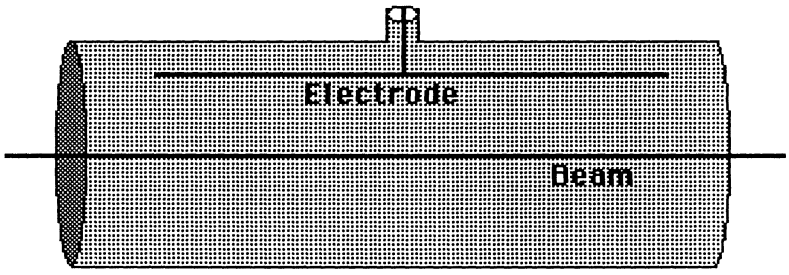

Fig. 9.1. Side view of an electrostatic pickup with the signal connection at the center. Because both ends are open, the beam can excite high-Q resonances in the electrode that have current nodes at the ends and a voltage node at the center.

The standard solution for minimizing the VSWR is to match the characteristic impedance of the electrode and the transmission line. In this case, the power induced on the electrode is transferred to the transmission line without any reflection and, therefore, appears immediately in the external circuit. This design is discussed in the following section.

10. DIRECTIONAL COUPLER PICKUP ELECTRODES

Directional coupler pickup electrodes (sometimes referred to as "stripline" or "microstrip" electrodes) are essentially transmission lines with a well-defined characteristic impedance and with a segment of the center conductor exposed to the beam.

We will examine the signal formation on this type of electrode in both the time and frequency domains. First, we consider the time domain.

Consider an electrode of azimuthal width ϕ, length ℓ, and characteristic impedance Z in a cylindrical beam pipe of radius b, as shown in Fig. 10.1. If the beam current is $I_b(t)$, the wall current intercepted by the electrode is $(\phi/2\pi) \bullet I_b(t)$ for a centered beam. This is the current that flows on the inner surface of the electrode exposed to the beam. When the beam pulse approaches the upstream end of the electrode, this wall current must cross the gap from the beam pipe wall to the electrode. Because the impedance of the gap is half the electrode's characteristic impedance (the inducing current sees two transmission lines in parallel), the voltage induced across the gap is $V(t) = (\phi/2\pi) \bullet (Z/2) \bullet I_b(t)$. This voltage then launches TEM waves in two directions. One signal goes out the upstream port to the electronics. The other wave travels down the outside surface (primarily) of the electrode to the downstream port at a signal velocity $v_s = \beta_s c$ and out the downstream port. Because the impedance of the transmission line is Z, the current flowing in each direction is half the current flowing on the inside surface of the electrode. The beam travels down the beam pipe at a velocity $v_b = \beta_b c$ and induces a similar signal at the downstream gap,

with a delay given by $\ell/\beta_b c$ and with opposite polarity to the first one. The net result is that at the upstream port, we see a bipolar-doublet signal of the form

$$V_U(t) = \frac{\phi Z}{4\pi}\left[I_b(t) - I_b\left(t - \frac{\ell}{\beta_b c} - \frac{\ell}{\beta_s c}\right)\right] \ ; \tag{10.1}$$

while at the downstream port, the bipolar signal is given by

$$V_D(t) = \frac{\phi Z}{4\pi}\left[I_b\left(t - \frac{\ell}{\beta_s c}\right) - I_b\left(t - \frac{\ell}{\beta_b c}\right)\right] \ . \tag{10.2}$$

If $\beta_b c$ equals the TEM wave velocity $\beta_s c$ on the electrode, there is complete cancellation at the downstream port. Therefore this form of electrode structure can be highly directional. Directivities (the ratio of forward to reverse power) close to 40 dB have been obtained. This is quite useful in monitoring beams in collider-type storage rings that have counter-rotating beams.

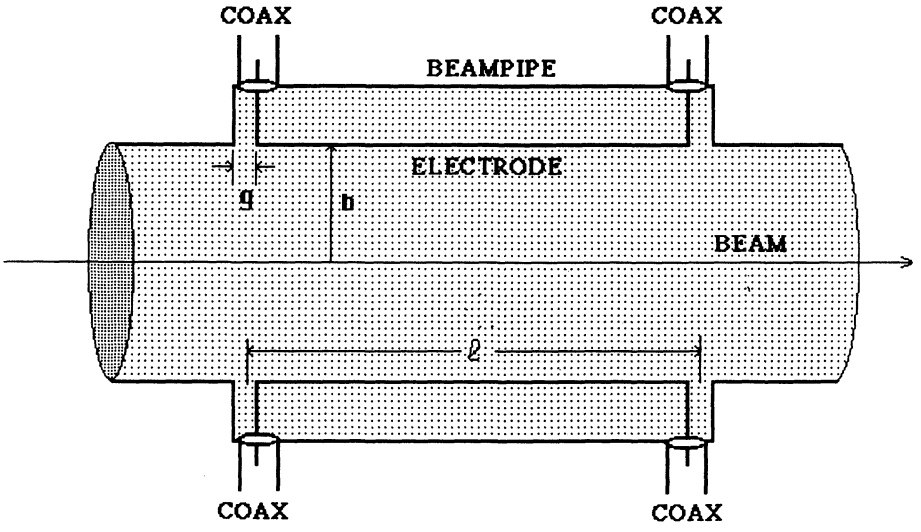

Fig. 10.1. Side view of a directional-coupler beam position electrode. The electrode is a section of an impedance-matched transmission line with the center conductor exposed to the image fields of the passing beam. Signals induced on the electrode exit through the upstream and downstream ports without reflection.

There are several variations of this geometry. In addition to terminating the downstream port in the characteristic impedance, the port may be either shorted to ground or left open. In these cases, the signal traveling down the

electrode to the downstream port is reflected, either inverted (shorted electrode) or noninverted (open electrode). In the latter case, a signal induced at the downstream port by the beam is twice the amplitude and the opposite polarity of the reflected signal. In all cases, the output signal at the upstream port is a bipolar doublet with zero net area.

For a Gaussian beam bunch shape, the bipolar doublet is of the form

$$V_U(t) = \frac{\phi Z}{4\pi}\left[\exp\left[\frac{-(t+\tau)^2}{2\sigma^2}\right] - \exp\left[\frac{-(t-\tau)^2}{2\sigma^2}\right]\right] I_b(t) \ , \tag{10.3}$$

$$\text{where } \tau = \frac{\ell}{2c}\left[\frac{1}{\beta_b} + \frac{1}{\beta_s}\right] \ . \tag{10.4}$$

This is plotted in Fig. 10.2 for a 10-cm-long electrode with several values of bunch length σ.

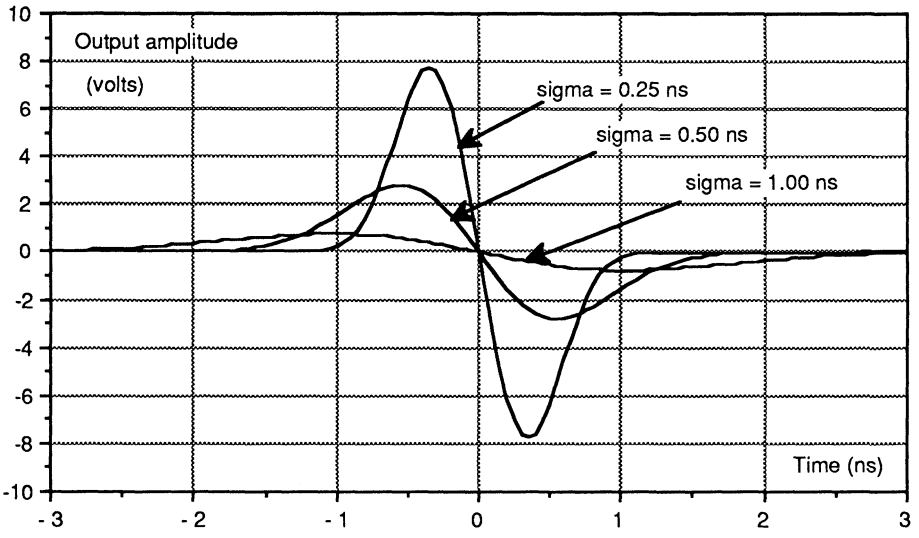

Fig. 10.2. Plot of the expected voltage waveform at the upstream port of a 10-cm-long, 45°-electrode 50 Ω directional-coupler pickup for 10^{10} protons with rms beam bunch lengths of 0.25, 0.5, and 1 ns.

The same analysis can be performed in the frequency domain using Eq. (4.4) for a beam current modulated at frequency $\omega/2\pi$. In this case the rms voltages at the upstream and downstream ports are

$$V_U(\omega) = \frac{\phi Z}{\sqrt{2}\pi}\langle I_b\rangle A(\omega)\,\sin\left[\frac{\omega\ell}{2c}\left(\frac{1}{\beta_s} + \frac{1}{\beta_b}\right)\right] \tag{10.5}$$

and

$$V_D(\omega) = \frac{\phi Z}{\sqrt{2}\pi}\langle I_b\rangle A(\omega)\,\sin\left[\frac{\omega\ell}{2c}\left(\frac{1}{\beta_s}-\frac{1}{\beta_b}\right)\right] \quad . \tag{10.6}$$

Note that there is a length of the electrode for which the argument of the sine function in Eq. (10.5) is $\pi/2$, and the output signal is maximized. This electrode is sometimes referred to as a "quarter wavelength" electrode, even though it is not quite quarter wavelength except when β_b and β_s are both equal to 1. Note also that there are periodic zeros in the response function when the argument is equal to $n\pi$. When this type of pickup is used as a wide-band pickup for looking at signals over a large frequency range, these dips in the response function are easily observed.

At low frequencies, the circular function in the expression for the signal amplitude at the upstream port can be replaced by its argument. The rms output voltage at low frequencies then becomes:

$$V_U(\omega) = \frac{\phi Z}{\sqrt{2}\pi}\langle I_b\rangle A(\omega)\frac{\omega\ell}{2\beta_b c}\left(1+\frac{\beta_b}{\beta_s}\right) \quad . \tag{10.7}$$

This approximation is valid if the electrode is substantially shorter than a quarter wavelength.

Comparing this approximation to Eq. (8.4) for the button electrode, we see that the two expressions are identical if the signal velocity β_s in Eq. (10.7) is set to infinity and R in Eq. (8.4) is set to $Z/2$. We have used two very different electrode designs in these calculations and two very different calculational methods. When a directional coupler electrode is very short, the output impedance does look like $Z/2$ (because it is terminated in Z at both ends), and we can also ignore the finite signal velocity on the electrode, so this equivalence is expected.

11. OTHER TYPES OF ELECTROMAGNETIC PICKUPS

There are several other types of electromagnetic position pickups that should be mentioned. Small loop couplers[22] (often called B-dot loops, meaning dB/dt) are simply small shorted antennas that couple to the azimuthal magnetic field of the passing beam and can be quite directional.

A second type of position pickup that has been used in the past is the "window frame" pickup electrode.[23] In this design, a ferrite window frame is linked with a conductor so that off-center beams create a difference signal.

A third type is the so-called slot coupler (Faltin pickup[24]) in which the beam fields couple to a nearby center conductor of a transmission line through holes or slots in the ground-plane wall, and induce signals that travel in the beam direction. One shortcoming of this design is that the slots make the transmission line dispersive, and the signal remains in synchronism with the beam for only a narrow frequency range.

A fourth type is a resonant rf cavity excited by a bunched beam in a TM mode that has a null for a centered beam. An off-center beam excites cavity resonances

whose amplitudes are proportional to the product of beam intensity × beam displacement and whose phase is dependent on the direction of displacement.[25]

12. HIGH-FREQUENCY EFFECTS

There are two high-frequency effects that the designer should consider when an electrode structure is being designed. These effects are the gap transit time and the Bessel factor.

If the gap g along the direction of the beam between the ground plane and the end of the electrode (see Fig. 10.1) is such that the transit time of the particle across the gap is a significant fraction of the period of the signal being measured, then the resultant signal amplitude is reduced by the transit time factor (TTF)

$$\text{TTF} = \frac{\sin \alpha}{\alpha} \quad ; \alpha = \frac{\omega g}{2\beta_b c} \quad . \tag{12.1}$$

The 3-dB point (TTF = 0.707) occurs when α in the above equation is about 1.4 radians (80°).

The Bessel factor arises from the fact that if the particle is not traveling at exactly the speed of light, the EM fields accompanying it are not TEM waves,[22] but have a finite longitudinal extent. This can be seen as follows. Consider a charged particle at rest and centered in a hollow conducting tube. In this case, the field lines connecting the particle to the tube have a finite longitudinal extent (along the axis of the tube), as shown in Fig. 12.1. The longitudinal distribution of charge on the inner wall of the hollow cylinder extends over about $b/\sqrt{2}$ (rms length) where b is the tube radius. If we now transform into a rest frame in which the particle is moving with a velocity $v_b = \beta_b c$, this longitudinal distribution of fields, and the corresponding wall current, moves with it. Note that the wall current actually precedes the particle. For highly relativistic particles, this longitudinal distribution of fields and corresponding wall currents contracts (Lorentz contraction) into a disk, i.e., a TEM wave with no z components. At high frequencies, this finite longitudinal extent causes the signals of slow particles ($\beta_b < 1$) to roll off with the (Bessel) factor BF

$$BF = \frac{1}{I_o(arg)} \quad ; \; arg = \frac{\omega b}{\beta_b \gamma_b c} \quad , \tag{12.2}$$

where $I_0(arg)$ is the modified Bessel function of order zero. For $arg = 0$, the Bessel factor is 1. The 3-dB point occurs for $arg = 1.22$. Good design practice generally limits arg to less than about 1.

As an example, consider a 1-MeV ($\beta_b = 0.046$) proton beam in a pickup with a 1 cm half-aperture. The 3-dB point occurs at about 270 MHz.

13. SIGNAL-TO-NOISE AND RESOLUTION

The available thermal noise power in a bandwidth B at temperature T is given by $P_N = kTB$ where k is Boltzmann's constant, T is the temperature in kelvin, and B is the bandwidth in hertz. This is about −114 dBm per MHz

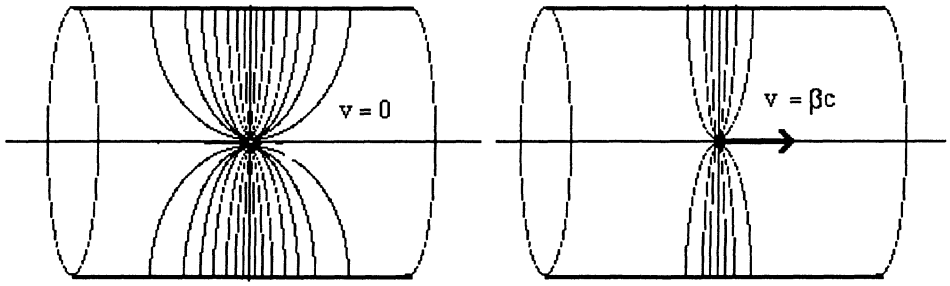

Fig. 12.1. The longitudinal field distribution of a static and moving charge ($\beta = 0.9$) in a grounded conducting cylinder. The longitudinal distribution contracts to a flat disk for highly relativistic particles. For slow particles, the field lines extend about $\pm b/\sqrt{2}$ longitudinally both in front of and behind the particle.

at room temperature. If we include the noise figure of the electronics, the noise power is often many decibels higher.

Resolution is sometimes limited by the noise power. We can use the relations developed in Eqs. (5.5) or (5.6) to estimate the resolution limit caused by thermal noise. The resolution limit is

$$\frac{\delta x}{b} = \frac{1}{4\sqrt{2}} \frac{\phi}{\sin(\phi/2)} \sqrt{\frac{P_N}{P_S}} \approx \frac{1}{2\sqrt{2}} \sqrt{\frac{P_N}{P_S}} \ , \tag{13.1}$$

where P_S is the signal power on a single electrode. Hence, a 40-dB signal-to-noise ratio (100:1 amplitude ratio) limits the resolution to about 0.35% of the half aperture.

As an example, consider a 1-mA beam in a quarter wavelength 45° (ϕ=0.79 radian), 50-Ω pickup. The signal power P_S per electrode at the upstream port of a directional coupler is given by

$$P_S = 2\left(\frac{\phi}{2\pi}\right)^2 Z\langle I_b\rangle^2 A^2(\omega) \sin^2\left[\frac{\omega\ell}{2c}\left(\frac{1}{\beta_b} + \frac{1}{\beta_s}\right)\right] \ . \tag{13.2}$$

Using the above parameters, $P_S = 1.56$ μW, which corresponds to −28 dBm. With a 10-MHz bandwidth and an electronic noise figure of 6 dB, the noise power P_N is −98 dBm. Thus the signal-to-noise ratio is about 70 dB, and the resolution limit is about 3 μm for a 50-mm-diam aperture.

Note that the signal power scales linearly with the characteristic impedance of the pickup, as is expected for current sources. Thus if signal-to-noise is a problem, raising the pickup impedance is a solution. Pickups with impedances exceeding 100 Ω have been used successfully. One way to accomplish this over a narrow band is to use a quarter-wave (transmission line) transformer at the

pickup to match the pickup to the cable. Resonant beam position monitors with effective electrode input impedances of approximately 5000 Ω have been made for measuring the position of very small beam currents.[26]

The RFI from accelerator rf systems can have serious effects on the accuracy and resolution if the shielding is not adequate. If the beam-bunching frequency is a subharmonic of the rf frequency, then operating the pickup at the lower frequency often eliminates the interference. EMI (electromagnetic interference) from pulsed and SCR power supplies is often a problem, and great care must be taken to eliminate ground loops that can pick up noise.

Shot noise is not a noise in the case of particle beams, but a signal. It relates specifically to fluctuations in the instantaneous beam current caused by the granularity of the individual particle charges. Because the fluctuations in beam current create a carrier signal, they allow detecting the beam position and therefore are sometimes called Schottky currents. The rms Schottky current for a coasting beam of average current $\langle I_b \rangle$ and bandwidth B is (for particles with charge $\pm e$)

$$I_{\text{shot}} = \sqrt{2e\langle I_b \rangle B} \quad . \tag{13.3}$$

A specific example is that the Schottky current for a 1-A proton beam with a 1-MHz bandwidth is 0.6 μA.

14. SIGNAL-PROCESSING METHODS

There are three general methods for deriving a normalized position signal from the raw pickup electrode signals. They are difference-over-sum (Δ/Σ) processing, amplitude-to-phase conversion (AM/PM) processing, and log-ratio processing. Each of these have certain advantages over the others. Specific advantages to look for are simplicity and cost, dynamic range (of beam signal intensity), linearity (of response vs displacement), and bandwidth (either acquisition or real-time).

Figure 14.1 shows the expected amplitude response using these three signal-processing methods for a 45° electrode width in a circular beam pipe. It is apparent that of the three processing methods, the log-ratio technique yields the response most linear in beam position.

15. DIFFERENCE-OVER-SUM PROCESSING

There are many variations of the difference-over-sum (Δ/Σ) method. We define shorthand notation as

$$\frac{\Delta}{\Sigma} = \frac{I_R - I_L}{I_R + I_L} \tag{15.1}$$

This ratio is "normalized," because it is independent of the beam current.

The simplest approach to obtain Δ/Σ would be to detect the rf signals using diode detectors, homodyne detectors,[27] or demodulator chips,[28] and then to generate analog signals proportional to the rf envelope amplitudes. These signals

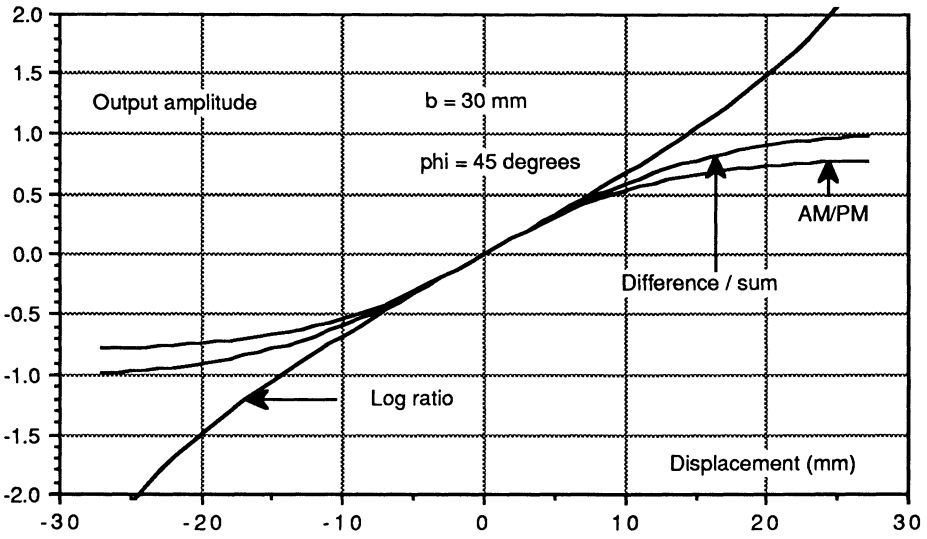

Fig. 14.1. Plot of the response of difference-over-sum, amplitude-to-phase conversion, and log-ratio processing methods to a displaced beam in a 60-mm-diam aperture with 45° directional-coupler electrodes. The log-ratio response is the most linear. All three curves have been normalized to the same slope at the center.

can then be digitized and then processed, or processed in analog circuits to achieve a Δ/Σ signal before digitization. Another common approach is to use 180° hybrid junctions to generate the Δ/Σ signal before rf detection. This latter method requires that the signals, and hence the signal cables, be properly phase-matched at the hybrid junction.

If the digitization is performed before the Δ/Σ function, the granularity of the ADC limits the dynamic range of the system. If the beam current varies over a 100 to 1 dynamic range (40 dB), the resolution with a 12-bit ADC is limited to about 2% of the half-aperture of the pickup at the low end. If the Δ/Σ function is performed in analog circuits, the analog-division process is slow and has a narrow dynamic range. An alternate process uses an automatic-gain-control (AGC) circuit as a normalizer.[29] This particular circuit also uses switching between electrodes at 40 kHz to eliminate possible gain differences between rf amplifier channels, which also limits the bandwidth.

One advantage to the Δ/Σ process is that it can also be carried out in the time domain by using a peak detector to capture the peak voltage in the bipolar signal from the individual electrodes.[30] A disadvantage of peak detection is that the peak voltage is very sensitive to the pulse shape, as is seen in Fig. 10.2. It is also very sensitive to cable attenuation and dispersion in long cables.[31] Of all

the processing methods, Δ/Σ is perhaps the easiest to implement, and therefore is by far the most popular method.

16. AMPLITUDE-TO-PHASE CONVERSION

In the amplitude-modulation-to-phase-modulation (AM/PM) method,[32] the two in-phase rf signals from the two pickup electrodes are split and re-combined in quadrature (i.e., with 90° relative phase shifts at the processing frequency) to convert the two signals of different amplitudes into two equal-amplitude signals whose phase difference is related to the amplitude difference of the two incoming signals. Figure 16.1 shows a block diagram of the basic conversion process, along with phasors indicating the signal processing. The transfer function is given by

$$\Delta\theta = 2\,\tan^{-1}\left(\frac{R}{L}\right) - \frac{\pi}{2} \tag{16.1}$$

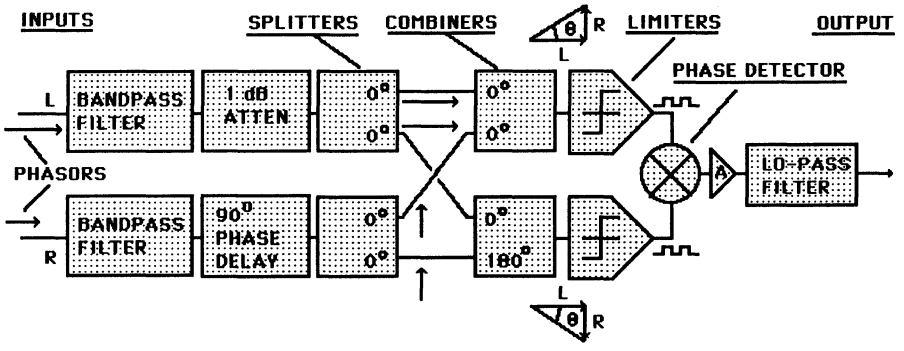

Fig. 16.1. Block diagram of the basic processing system for amplitude-to-phase conversion. After the two in-phase signals are filtered, they are split and recombined in quadrature using power splitters and combiners. At this point, the amplitude difference of the two input signals has been converted to a phase difference (6.6° per dB). The limiters remove the amplitude variation while preserving the phase information. The phase detector produces an analog signal proportional to the phase difference.

The conversion gain for these circuits is typically 6.6° of phase shift for each decibel of amplitude difference in the incoming signals. The quadrature phase shift can be accomplished by using either quarter-wavelength transmission lines (least expensive, but limited to a single frequency) or quadrature hybrids. The two signals are then clipped to a constant amplitude in a hard-limiter circuit that preserves the phase information within a fraction of a degree but removes all amplitude dependence, and then the phase difference is measured in a phase-detector circuit. The most common hard limiter presently in use is the 9685-type comparator, and the phase detectors are usually double-balanced mixers or exclusive ORs.

The analog voltage output of the AM/PM processor is related to the amplitudes R and L of the two input signals by the relation

$$V_{\text{out}} = V_o\left[\tan^{-1}\left(\frac{R}{L}\right) - \frac{\pi}{4}\right] = V_o \tan^{-1}\left(\frac{R-L}{R+L}\right) \quad . \tag{16.2}$$

Note the relationship to the Δ/Σ processing algorithm.

Hard limiters are usually the components that most restrict the system performance. Their dynamic range varies from 40 to over 60 dB depending on the operating frequency. They have been used at frequencies up to 100 MHz but perform best below about 20 MHz. To use hard limiters when the beam-current modulation is over 100 MHz, the rf signal is often heterodyned down to a lower frequency, typically 10 or 20 MHz. The real-time bandwidth is about 10% of the processing frequency and can be as high as 10 MHz.

AM/PM circuits using down conversion from 200 to 10 MHz and 425 to 20 MHz have been built at Los Alamos.[33] Fermilab has built approximately five hundred 53-MHz units and has built down-conversion units for both the 200-MHz proton linac and for the rapid-cycling Booster synchrotron.[34] This latter application is quite interesting in that the local oscillator used for the down-conversion tracks the Booster rf frequency from 30 to 53 MHz with a constant frequency offset, so that the IF frequency output to the AM/PM circuit is constant.

It is essential to keep the relative phase of the two signals entering the AM/PM processor within about $\pm 5°$, otherwise Eq. (16.1) must be modified. Phase matching of the cables from the pickups to the electronics is therefore required.

The AM/PM circuits are specifically for frequency-domain signal processing and therefore function well for multibunch beam pulses. AM/PM processing has also been used for the measurement of the position of single, isolated beam bunches. In this application, a narrow-band filter is placed upstream of the AM/PM processor. The passage of a single bunch by the pickup electrode shock-excites the bandpass filter to ring for perhaps 10 cycles, which is sufficient time to complete the phase difference measurement.[21, 32] These filters must be very carefully matched, with center frequencies equal within about $\pm 0.1\%$. Both lumped-component circuits and shorted coaxial transmission lines have been used in this application.

Real-time bandwidth is important if the signal is to be used in real-time control of the beam position. In this case, the processed beam position signal is fed back to a beam deflector electrode located upstream of the pickup, and the system is run in closed-loop fashion to reduce the transverse beam jitter. Because AM/PM system provides a normalized position signal, the position signal is independent of beam intensity. The jitter-control function can be accomplished more simply by using an unnormalized difference signal if the beam intensity variation is minimal. In this case, the closed-loop gain is proportional to the beam intensity.

Of the three basic types of position processors reviewed here, the AM/PM circuit is the most expensive and difficult to implement. However, the obtainable large dynamic range and high real-time bandwidth are very desirable features. Thus far, their application is limited to the Linac, Booster, Main Ring, and Tevatron[35] at Fermi National Accelerator Laboratory (FNAL); the Proton Storage Ring at Los Alamos National Laboratory;[36] and the LEP ring[21] at CERN. The HERA-P ring at DESY also is planning to use a similar circuit. The SLAC SLC arcs[37] use Δ/Σ, however.

If ultimate resolution is the main objective, it is important to consider the effective noise figures obtainable with the various circiuts. The effective noise figure for the electronics at the input of the hard limiter in AM/PM processing is in the 10- to 20-dB range and, in addition, there is noise downstream of the hard limiter that produces a resolution minimum independent of beam current.

17. LOG-RATIO PROCESSING

In the log-ratio method, the two signals are put into a discrete or hybrid circuit that produces an output signal proportional to the logarithm of the ratio of the two input signals. The log function is usually obtained by using an ideal forward-biased diode junction in the feedback circuit. There are several limitations to this method. First, commercial circuits are limited to a few hundred kilohertz of bandwidth because of the high dynamic resistance of the "diodes" (actually the base-emitter junctions of matched transistors) at low currents in combination with the distributed capacitance. A circuit designed for high-bandwidth operation possibly could achieve a bandwidth approaching 10 MHz. Second, the log-ratio circuit inputs are usually unipolar, so the signals must be the detected-envelope signals rather than the raw rf signals. Third, the output signal amplitude is proportional to the absolute temperature of the diode junction and should be temperature-compensated. The Analog Devices[38] AD538 is a commercially available log-ratio chip with temperature compensation. The Analog Devices AD540 chip uses controlled gain compression to emulate the log process and has bandwidths approaching 100 MHz.

The output of the log-ratio circuit is proportional to

$$V_{\text{out}} = V_o \, Ln\left(\frac{R}{L}\right) = 2V_o \, \tanh^{-1}\left(\frac{R-L}{R+L}\right) \tag{17.1}$$

Note the similarity to both the Δ/Σ and the AM/PM algorithm.

18. INTENSITY MEASUREMENT

Although the pickups and circuits discussed here are primarily designed for position measurement, they can be used to measure beam intensity as well. An example of this is the beam position system in the FNAL Tevatron, which has about 220 beam position monitors evenly distributed around the ring (mostly at 4 kelvin because the machine is superconducting) and only one beam current monitor. During the commissioning process, the ability to measure the beam

intensity at every beam position monitor (using the sum of the electrode signal amplitudes) with a few percent accuracy was absolutely necessary to obtain the first full revolution of beam. Because the output power of the summed signal is slightly sensitive to both the beam bunch length and the beam position, the accuracy is limited.

19. ALIGNMENT, CALIBRATION, AND ON-LINE TESTING

The initial alignment and calibration can be separated into three main components: the pickup electrode assembly, the cabling, and the electronics.

After the pickup construction and assembly is complete, the electrode assembly is normally first "mapped" with an rf-excited taut wire stretched through the pickup at specific points to determine the electrical response for various displacement values of x and y, to determine both the electrical center and the displacement sensitivities, as well as the nonlinearities.[19] The pickup is then installed and aligned mechanically with the other beamline components. An optional alternative is to place the taut wire along the magnetic axis of the beamline magnetic optics after the pickup is mechanically mounted, excite the wire with an rf signal, then measure the electrical offset (decibels of output signal unbalance) relative to the magnetic, rather than the mechanical, axis of the beam optics.[39] The electrical offset and the displacement sensitivity are then put into the computer database for correction to the beam position data as they are read out. The nonlinearities, as shown in Fig. 14.1, can be corrected in a look-up table at this time.

In the taut-wire measurement, the signal on the wire is by definition a TEM (principal) wave with no longitudinal electric or magnetic component, travels at the velocity of light, and emulates highly relativistic particles. The signals associated with slow particles, as discussed in Sec. 12 and illustrated in Fig. 12.1, are very difficult to generate on wires. As was shown in Secs. 6 through 10, the pickup response depends on the particle velocity, and this must be taken into account when calculating the pickup response.

The coax cables connecting the pickup electrode to the electronics must be checked for attenuation. If the signal processing is dependent on the relative phase delay in the cable pairs, their electrical length must be equalized as well.

The electronics can be separately calibrated for any electrical offset in output reading and in the voltage output vs decibel difference between the two inputs at a variety of fixed signal input power levels. Because the electronics is an active circuit, it can be expected to have nonlinearities. Therefore the electronics needs to be "aligned" before installation. The alignment process can be quite cumbersome if performed manually, so it is often performed using a computer-automated system. A common alignment circuit in use at both FNAL and LANL is an rf signal generator that uses electronic attenuators under computer control to step through a variety of input unbalances (-10 dB to $+10$ dB in 1-dB steps, and from -60 dBm to 0 dBm in total power output in 1-dB steps (a total of 1260 settings) in about 100 ms.[33] The electronic unit also provides a z axis and a horizontal axis signal (linear in total power dBm) to an x-y oscilloscope. The

analog output of the position-processing electronics provides the y-axis signal. The oscilloscope display is thus a real-time raster display with a 10-Hz refresh rate.

The overall calibration of assembled systems is of the order of 0.5% to 1% of the full aperture for center position accuracy and about ±2% on the displacement sensitivity S_x. Resolution can approach the signal-to-noise limit in Eq. (13.1).

Equally important is providing some way in which to monitor the performance and calibration of a system while it is in use. A method used at FNAL provides special test inputs into the rf input ports of the electronics that could perform these tests. A 10-mA dc current was put through a high-frequency inductor and onto the upstream side of a dc isolator in the rf circuitry. Because the pickup electrodes were back-terminated directional couplers, a measurement of the dc voltage at the point of current input determined the back-termination value within a few ohms and that continuity existed through the signal cable and the directional coupler (at 4 kelvin in the Tevatron) to the back terminations. The same test ports allowed injection of rf signals through a capacitive coupling into the signal-processing electronics with several decibel ratios to check proper operation of the electronics. All these tests, as well as the digitizers for collecting the measurement data, were under local microprocessor control, and the measured data was stored in RAM for subsequent readback by the host computer.

The degree of automation required depends on the size of the position measurement system, and the remoteness of the system components from the central computer. Because beam position measuring systems normally do not have redundancy, it is important to be aware of any channels that are not operating properly.

20. GENERAL HARDWARE SYSTEM ARCHITECTURE

More often than not, accelerator control systems, of which the beam diagnostics systems are an integral part, utilize distributed intelligence to control, read back, and perform a set of on-line tests on the systems that interface to the accelerator.

There are several advantages to using distributed intelligence. First, if a particular diagnostic subsystem performs a critical protection function on an accelerator component, the subsystem must remain operational even when the network to the host computer fails. Second, the microprocessor contains in its database the programs for performing the data collection tasks and the on-line calibration tasks, which can be initiated by the host and performed without host intervention.

In small, local systems, such complexity is not needed. An issue that always seems to arise in the design of small systems is whether the simultaneous measurement of beam position at many position pickups is required. It is certainly much less expensive to install multiplexers and sequentially process the signals from different pickups. However, if the accelerator has a very low duty cycle and a low repetition rate, data collection can be very slow with

a multiplexed system. Also, if it is important to record betatron oscillations around the closed orbit in a synchrotron for "tune" or betatron phase advance information, a nonmultiplexed system is much preferable.

In terms of interconnections to the host, the following scheme was found to be quite efficient at the Tevatron.[40] A high-speed communication network (in this case serial CAMAC) was used as a point-to-point bidirectional link for downloading control parameters and reading back data asynchronously (not in real time but under the control of the host). A second single coaxial cable carried a 10-MHz bipolar clock signal with a set of superimposed diphase-encoded timing signals simulataneously to all microprocessors to synchronize them and to initiate sample-and-hold gating and digitization of beam position information or on-line system tests. The results were then stored in local memory until the host requested it. This minimized the traffic on the computer network.

21. SOFTWARE AND DISPLAYS

The effort put into developing software and displays always seems to be underestimated. Creative programmers never seem to have sufficient time to implement their plans. There is however, a minimum amount of software that is truly necessary. It usually is very unique to the specific application and cannot be specified adequately without a detailed knowledge of the system requirements.

Nevertheless, it is possible to say a few words about certain common aspects of software and displays. Automatic beamline control by closing the control loop from the position pickup to beam steering devices through the host computer is becoming more necessary as accelerators and beamlines become more complex. It simply is not possible to steer a beam through a long, complex beamline, or to minimize the orbit distortions in a large synchrotron, without the support of software algorithms.[41,42] In some beamlines, it may be more accurate to measure the magnetic-lattice transfer matrices on-line than to compute them from beamline lattice designs.

In another area, the need for archiving measurement data for later recall in order to make comparisons is very important in locating malfunctioning accelerator components. For example, "cusps" in the orbit distortions that pinpoint the orbit perturbation are determined by subtracting archived data from new data for the same accelerator operating conditions. Another application is making specific measurements that require changing the accelerator operating conditions; (e.g., making measurements of the dispersion in the lattice[43]). A third reason for archiving on a very short-term basis is to store a series of beam position measurements in FIFO memories thereby making available instant replays of accelerator performance just before unexpected equipment failures and subsequent beam loss. This of course represents a tremendous amount of data and certainly cannot be handled over a network. For this reason, such a capability must be built into the distributed intelligence, local to the beam position electronics.

Having the right software and displays available at turn-on is a tremendous asset in commissioning a facility. The software is usually one of the last

components to be "installed," and as often as not, it is written by a programmer who is unfamiliar with the accelerator and therefore does not write programs that provide the displays and other information in the most useful format for presentation. Furthermore, as distributed intelligence is becoming more common, the software "tree" is becoming multitiered in that specific control and data-processing functions are being separated into various locations, often with different operating systems, programming languages, and even programmers.

22. CONCLUSIONS

In designing a beam position measurement system, it is important to understand fully the characteristics of beam position diagnostics devices and the accelerator facility in which they are to be installed. It is possible to build a technically excellent piece of hardware that relies on the presence of beam modulation signals that are not always present, or does not take into account all the possible operating conditions of the accelerator, and therefore does not always provide the required measurements. In short, the designer must be knowledgeable in all aspects of the accelerator operation, the beam-coupling mechanism to the pickup electrodes, electronic instrumentation design, and in the applications software.

23. REFERENCES

1. J. Borer and R. Jung, "Diagnostics," CERN Publication 84-15, 385 (1984).

2. G. Lambertson, "Dynamic Devices; Pickups and Kickers," AIP Conf. Proc. **153**, M. Month, Ed., 1413 (1987).

3. R. Littauer, "Beam Instrumentation," AIP Conf. Proc., **105**, M. Month, Ed., 869 (1983).

4. R. H. Siemann, "Bunched Beam Diagnostics," AIP Conf. Proc. **184**, M. Month, Ed., 430 (1989).

5. J. L. Pellegrin, "Review of Accelerator Instrumentation," Proc. XI*th* International Conf. on High-Energy Accelerators, CERN, 459 (1980).

6. "Frontiers of Particle Beams; Observation, Diagnosis, and Correction," Proc. of the Joint U.S. CERN School on Particle Accelerators, M. Month and S. Turner, Eds., Capri, 1988, Springer Verlag Lecture Notes in Physics **343** (1989).

7. C. D. Moore et. al.; "Single Bunch Intensity Monitoring System Using an Improved Wall Current Monitor," Proc. 1989 Particle Accelerator Conf., IEEE Catalog No. 89CH2669-0, Chicago, IL, 1513 (1989). See also R. Webber, these proceedings.

8. R. Jung, "Beam Intercepting Monitors," Ref. 6, page 403.

9. R. J. Nawrocky et al., "Automatic Control of Position and Direction of X-Ray Beams at NSLS," Proc. 1989 Particle Accelerator Conf., IEEE Catalog No. 89CH2669-0, Chicago, IL, 1856 (1989).

10. D. D. Chamberlin, "Imagescope to Photodiode Beam Profile Imaging System," IEEE Trans. Nucl. Sci. **30**, 2201 (1983).

11. F. Hornstra, "Residual Gas Ionization Profile Monitor for HERA," Proc. European Particle Accelerator Conference, Rome, 1160 (1988).

12. C. Field, "Problems of Measuring Micron Size Beams," Proc. 1989 Particle Accelerator Conf., IEEE Catalog No. 89CH2669-0, Chicago, IL, 60 (1989).

13. R. Ericson, "Monitoring in Future e^+e^- Colliders," Ref. 6, page 482.

14. W. B. Cottingame et al., "Noninterceptive Monitoring of Longitudinal Parameters in H^- Beams," IEEE Trans. Nucl. Sci. **32**, 1871 (1985).

15. M. Placiti and R. Rossmanith, "e^+e^- Polarimetry at LEP," Nucl. Instr. and Meth. **A274**, 79 (1989).

16. W. Barry, R. Rossmanith, and M. Wise, "A Simple Beam Position Monitor System for CEBAF," 1988 Linear Accelerator Conference Proceedings, CEBAF-Report-89-001, 649 (1989). See also P. Adderley et al., "A Beam Monitor for Low Intensity Beams," Proc. 1989 Particle Accelerator Conf., IEEE Catalog No. 89CH2669-0, Chicago, IL, 1602 (1989).

17. R. E. Shafer, "Characteristics of Directional Coupler Beam Position Monitors," IEEE Trans. Nucl. Sci. **32**, page 1933 (1985).

18. K. Satoh, "Beam Position Monitor using Wall Currents," Rev. Sci. Instr. **4**, 450 (1979).

19. W. Schutte, "Results of Measurements on the HERA Proton Beam Monitors," Proc. 1989 Particle Accelerator Conf., IEEE Catalog No. 89CH2669-0, Chicago, IL, 1471 (1989).

20. T. Linnecar, "High Frequency Longitudinal and Transverse Pickups used in the SPS," CERN SPS/ARF/78-17 (1978).

21. J. Borer et al., "LEP Beam Orbit System," Proc. 1987 Particle Accelerator Conf., IEEE Catalog No. 87CH2387-9, 778 (1988).

22. J. H. Cuperas, "Monitoring of Beams at High Frequencies," Nucl. Instr. and Meth. **145**, 219 (1977).

23. J. Claus, "Magnetic Beam Position Monitor," Proc. IEEE Particle Accelerator Conference, NS-20, **3**, 590 (1973).

24. L. Faltin, "Slot-Type Pickups," Nucl. Instr. and Meth. **148**, 449 (1978).

25. J. McKeown, "Beam Position Monitor using a Single Cavity," IEEE Trans. Nucl. Sci. **26**, 3423 (1979). See also ibid. **28**, 2328 (1981).

26. Q. Kerns et al., "Tuned Detector for Fermilab Switchyard," Proc. 1987 Particle Accelerator Conf., IEEE Catalog No. 87CH2387-9, 661 (1988).

27. R. Bossart et al., "Synchronous Receivers for Beam Position Measurement," IEEE Trans. Nucl. Sci. **32**, 1899 (1985).

28. J. Hingston, J. Johnston, and I. Ko, "Advanced Light Source (ALS) Beam Position Monitor," Proc. 1989 Particle Accelerator Conf., IEEE Catalog No. 89CH2669-0, Chicago, IL, 1507 (1989).

29. R. Biscardi, J. W. Bittner, "Switched Detector for Beam Position Monitor," Proc. 1989 Particle Accelerator Conf., IEEE Catalog No. 89CH2669-0, Chicago, IL, 1516 (1989).

30. R. E. Meller, D. Sagan, and C. R. Dunnam, "Beam Position Monitors for the CESR Linac," Proc. 1989 Particle Accelerator Conf., IEEE Catalog No. 89CH2669-0, Chicago, IL, 1468 (1989).

31. The skin effect causes both the signal attenuation and the signal velocity to have a square-root-of-frequency dependence. The attenuation in nepers is equal to the phase shift in radians (i.e., 1 dB of attenuation corresponds to 6.6° of phase shift).

32. S. P. Jachim, R. C. Webber, and R. E. Shafer, "RF Beam Position Measurement for Fermilab Tevatron," IEEE Trans. Nucl. Sci. **28**, 2323 (1981).

33. F. D. Wells and S. P. Jachim, "A Technique for Improving the Accuracy and Dynamic Range of Beam Position Monitors," Proc. 1989 Particle Accelerator Conf., IEEE Catalog No. 89CH2669-0, Chicago, IL, 1595 (1989).

34. R. Webber et al., "Beam Position Monitoring for the Fermilab Booster," Proc. 1987 Particle Accelerator Conf., IEEE Catalog No. 87CH2387-9, 541 (1988).

35. R. E. Shafer, R. E. Gerig, A. E. Baumbaugh, and C. R. Wegner, "Tevatron Beam Position and Beam Loss Monitor Systems," Proc. XII*th* International Conf. on High-Energy Accelerators, Fermi National Laboratory, 609 (1983).

36. E. F. Higgins and F. D. Wells, "A Beam Position Monitor System for the Proton Storage Ring at LAMPF," IEEE Trans. Nucl. Sci. **28**, 2308 (1981).

37. J. L. Pellegrin and M. Ross, "Beam Position for SLAC SLC Arcs," Proc. 1987 Particle Accelerator Conf., IEEE Catalog No. 87CH2387-9, 673 (1988).

38. Analog Devices Inc., Two Technology Way, Norwood, MA 02062.

39. Q. Kerns et al., "RF Precision Alignment of Beam Position Monitors in Tevatron," IEEE Trans. Nucl. Sci. **30**, 2250 (1983).

40. R. J. Ducar, J. R. Lackey, and S. R. Tauser, "FNAL Synchronization Control for Collider Operation," Proc. 1987 Particle Accelerator Conf., IEEE Catalog No. 87CH2387-9, 1937 (1988).

41. J.-P. Koutchouk, "Trajectory and Closed Orbit Correction," Reference 6, page 46 (1989).

42. R. Raja, A. Russell, and C. Ankenbrandt, "The Tevatron Orbit Program," Nucl. Instr. and Meth. **A242**, 15 (1985).

43. R. E. Shafer, "Beam Diagnostics at the Tevatron," IEEE Trans. Nucl. Sci. **32**, 1862 (1985).